European Radiology (2020) 30:5130–5138
https://doi.org/10.1007/s00330-020-06890-x

MAGNETIC RESONANCE

Respiratory motion–resolved four-dimensional zero echo time (4D ZTE) lung MRI using retrospective soft gating: feasibility and image quality compared with 3D ZTE

Kyungsoo Bae[1,2] · Kyung Nyeo Jeon[1,2] · Moon Jung Hwang[3] · Joon Sung Lee[3] · Sung Eun Park[1,2] · Ho Cheol Kim[4] · Anne Menini[5]

Received: 2 January 2020 / Revised: 18 March 2020 / Accepted: 10 April 2020 / Published online: 24 April 2020
© European Society of Radiology 2020

Abstract

Objectives To evaluate the feasibility and image quality of respiratory motion–resolved 4D zero echo time (ZTE) lung MRI compared with that of 3D ZTE.

Methods Our institutional review board approved this study. Twenty-one patients underwent lung scans using 3D ZTE and 4D ZTE sequences via prospective and retrospective soft gating techniques, respectively. Image qualities of 3D ZTE and 4D ZTE at end-expiration were compared through objective and subjective assessments. The quality of end-expiratory images of 3D ZTE and 4D ZTE of the two groups with different lung functions was also compared.

Results Images were successfully acquired in all patients without any adverse events. Signal-to-noise ratios (SNRs) of lung parenchyma and thoracic structures were significantly (all $p < 0.001$) higher in 4D ZTE. Contrast-to-noise ratios (CNRs) of peripheral bronchi, peripheral pulmonary vessels, and nodules or masses were significantly (all $p < 0.001$) higher in 4D ZTE. The subjective image quality assessed by two independent radiologists showed that intrapulmonary structures, noise and artifacts, and overall acceptability were superior in 4D ZTE (all $p < 0.001$). Image qualities of groups with normal and low lung functions differed significantly (all $p < 0.05$) in 3D ZTE, but not in 4D ZTE. The mean acquisition time was 136 s (127–143 s) in 3D ZTE and 325 s (308–352 s) in 4D ZTE.

Conclusions Respiratory motion–resolved 4D ZTE lung imaging was feasible as part of routine chest MRI. The 4D ZTE provides motion-robust lung parenchymal images with better SNR and CNR than the 3D ZTE, regardless of patients' lung function.

Key Points

- *ZTE MRI captures rapidly decaying transverse magnetization in the lung parenchyma.*
- *4D ZTE provides motion-robust lung parenchymal images with better SNR and CNR compared with 3D ZTE.*
- *Compared with 3D ZTE, the image quality of 4D ZTE lung MRI was affected less by patients' lung function and respiratory performance.*

Keywords Lung · Magnetic resonance imaging · Respiration · Organ motion · Cine MRI

Electronic supplementary material The online version of this article (https://doi.org/10.1007/s00330-020-06890-x) contains supplementary material, which is available to authorized users.

✉ Kyung Nyeo Jeon
knjeon@gnu.ac.kr

[1] Department of Radiology, Institute of Health Sciences, School of Medicine, Gyeongsang National University, Jinju, South Korea

[2] Department of Radiology, Gyeongsang National University Changwon Hospital, 555 Samjeongja-dong, Seongsan-gu, Changwon, South Korea

[3] General Electric (GE) Healthcare Korea, Seoul, South Korea

[4] Department of Internal Medicine, School of Medicine, Gyeongsang National University, Jinju, South Korea

[5] Applied Science Lab, GE Healthcare, Menlo Park, CA, USA

Abbreviations

CNR	Contrast-to-noise ratio
RF	Radio frequency
ROI	Region of interest
SI	Signal intensity
SNR	Signal-to-noise ratio
UTE	Ultrashort echo time
ZTE	Zero echo time

Introduction

Magnetic resonance imaging (MRI) of the lung is beneficial to patients requiring frequent follow-up examinations due to its non-ionizing character. However, the physical properties of lung hamper widespread clinical application of MRI. The low proton density and the short T2 of lung parenchymal tissue require rapid data sampling after RF pulse and maximum *k*-space coverage during the acquisition time limited by ultra-short T2*. Newly introduced short T2–sensitive techniques such as ultrashort echo time (UTE) and zero echo time (ZTE) sequences can satisfy these requirements [1, 2]. UTE sequence is effective in detecting and characterizing lung parenchymal diseases [3–8]. With an echo time (TE) of less than 100 μs in UTE, the short T2* of lung tissue offers limited constraint. Recently, respiratory-gated 3D UTE has been used for high-resolution imaging of the lung [9].

As another technique that can image tissues with ultrashort T2/T2*, ZTE sequence has been introduced in lung MRI [10, 11]. As the dead time between RF excitation pulse and data acquisition is a nominal zero, rapidly decaying transverse magnetization in the lung parenchyma can be effectively captured using this sequence. According to a recent study comparing 3D UTE and ZTE lung MR images, ZTE is better than UTE for the detection of lung parenchymal signal and visualization of intrapulmonary structures when optimized parameters are used for each sequence [12].

The structural lung MRI using UTE or ZTE is performed via respiratory gating during free breathing to acquire more radial projections and resolve the effect of respiratory motion [11, 13]. In spite of respiratory gating, image blurring is common in lung MR, especially in patients with inconsistent respiratory pattern, which can be addressed by retrospective soft gating in which the respiratory motion compensation is processed computationally during image reconstruction [14]. By adding a motion dimension to volume data using retrospective soft gating, dynamic 3D (or four-dimensional (4D)) MR images could be generated to obtain functional information. The feasibility of respiratory motion–resolved 4D lung imaging using UTE sequence has been demonstrated via clinical research [15]. Motion-resolved 4D ZTE lung imaging has been proposed and demonstrated in two volunteers [16]. However, the applicability of 4D ZTE in clinical chest MRI and the quality of 4D ZTE lung images have yet to be reported. The goal of this study was to evaluate the feasibility of 4D ZTE lung imaging during routine chest MRI, especially in patients with poor respiratory performance. We also assessed the image quality of 4D ZTE lung MRI compared with that of 3D ZTE.

Materials and methods

Patients

Our institutional review board approved this study. Written informed consent was obtained from all patients. From Oct. 2018 to Mar. 2019, 21 patients who underwent chest MRI for further evaluation of lung ($n = 15$), mediastinal ($n = 4$), or chest wall ($n = 2$) lesions detected on CT were enrolled. The study included 15 males and 6 females with a mean age of 65 years (range, 19–88 years). Pulmonary function test results were available for all patients. Since 3D ZTE lung scan has been performed as a part of routine chest MRI protocol at our institution, the 4D ZTE lung MRI was additionally performed during the same scanning session. Based on pulmonary function test and clinical assessment, 12 patients had normal lung function and 9 patients showed low lung function (obstructive pattern).

Image acquisition

MR images were obtained using a commercial 3-T scanner (Signa Architect, GE Healthcare) with a 16-channel body anterior array coil and a 40-channel posterior array coil. The ZTE sequence consists of a non-selective hard pulse excitation followed by 3D center-out radial sampling (Fig. 1). The 3D and 4D ZTE lung scans were performed consecutively during quiet breathing. A commercially available respiratory bellows (GE Healthcare) was wrapped around the patient's upper abdomen. Signals of the respiratory bellows were used as surrogates of respiratory motion. Scan parameters of 3D ZTE and 4D ZTE are summarized in Table 1.

Respiratory gating and image reconstruction

In 3D ZTE, a prospective respiratory gating technique was used for data acquisition. Data were prospectively acquired only when the position of the diaphragm was within an acceptance window during approximately one third of end-expiration phase. In 4D ZTE, a retrospective soft gating method was used for motion correction and image reconstruction as follows. *k*-space data along with physiological signals derived from respiratory bellows were collected during the whole respiratory cycles. The *k*-space data were binned into four respiratory motion states based on physiological signals.

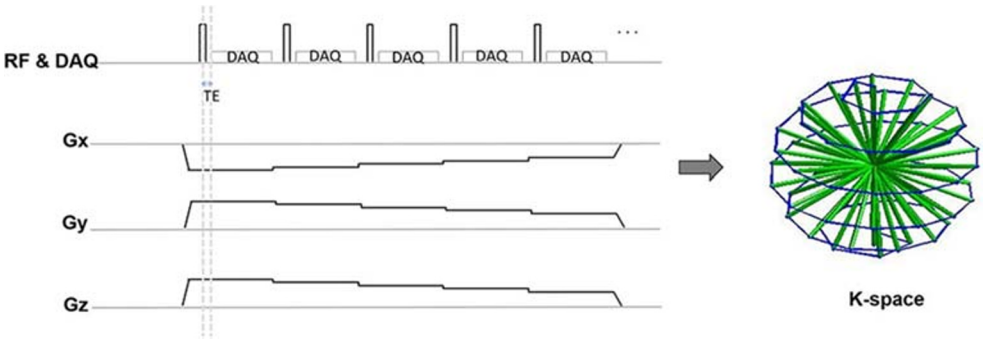

Fig. 1 Diagram of ZTE MR sequence showing an example of five spokes in one segment. Note that readout gradients are already ramped up before RF pulse. Non-selective hard pulse excitation is followed by 3D center-out radial sampling

For each respiratory motion state, the *k*-space data were weighted depending on the respiratory displacement from an ideal target physiological signal. The corresponding image volume was then reconstructed. Figure 2 shows differences in data acquisition and the *k*-space between 3D ZTE and 4D ZTE. Coronal images with an isotropic resolution of 1.4 mm were obtained in both sequences. Original coronal image data of 4D ZTE and 3D ZTE were reformatted into axial images. While only a single image dataset was generated for 3D ZTE, four image datasets were generated in 4D ZTE according to the different respiratory motion states (phase 1, beginning of inspiration ~ phase 4, end-expiration) (Fig. 3).

Image analysis

All images were reviewed and analyzed with a PACS system (Universal Viewer 6.0; GE Healthcare). Image analysis and comparison were performed using end-expiratory image datasets in both sequences. The 3D ZTE image dataset consisted of prospective images acquired at approximately one third of the end-expiration phase of respiratory cycles (blue area in Fig. 2a). Among the four retrospective datasets acquired during whole respiratory cycles in 4D ZTE, an image dataset acquired at one fourth of end-expiration phase (phase 4, blue area in Fig. 2c) was used.

Quantitative evaluation

Signal intensities (SIs) of lung parenchyma and normal structures were measured for the comparison of 3D ZTE and 4D ZTE. One radiologist (with 6 years of experience) drew circular regions of interest (ROIs) in the lung parenchyma, tracheal lumen, tracheal wall, peripheral bronchus, peripheral pulmonary vessel, aorta, and subscapularis muscle on each image dataset (Fig. 4). In patients with parenchymal nodule or mass, the signal of nodule or mass was also measured. All measurements were performed three times, and the mean was recorded as the representative value. The size of the ROI was adapted to the diameter of the structure. The same size was used for the same location in both sequences. When measuring the SI of the lung, vascular markings and fissures were avoided. For the SI of the trachea, the ROI was placed in the anterior or lateral tracheal wall without including luminal air. For the peripheral pulmonary vessel, the circular ROI was drawn on a segmental pulmonary vessel appearing round on the axial image while avoiding the adjacent lung. In the peripheral bronchus, after

Table 1 Scan parameters of 3D and 4D ZTE lung MR images in 21 patients

	3D ZTE	4D ZTE
Acquisition type	3D, coronal	
FOV (isotropic)	384 × 384 mm	
Frequency	256	
Slice thickness	1.4 mm	
Number of slices	160–180 depending on the patient volume	
Number of motion-resolved datasets	1	4
Acquisition resolution	1.4 mm isovoxel	
Receiver bandwidth	± 31.25 kHz	
Flip angle	2°	
No. of spokes per segment	256	
Gating	Prospective gating	Retrospective soft gating
Respiration trigger window	30	N/A
Scan time (mean, range)	127 s (125–136 s)	325 s (308–352 s)

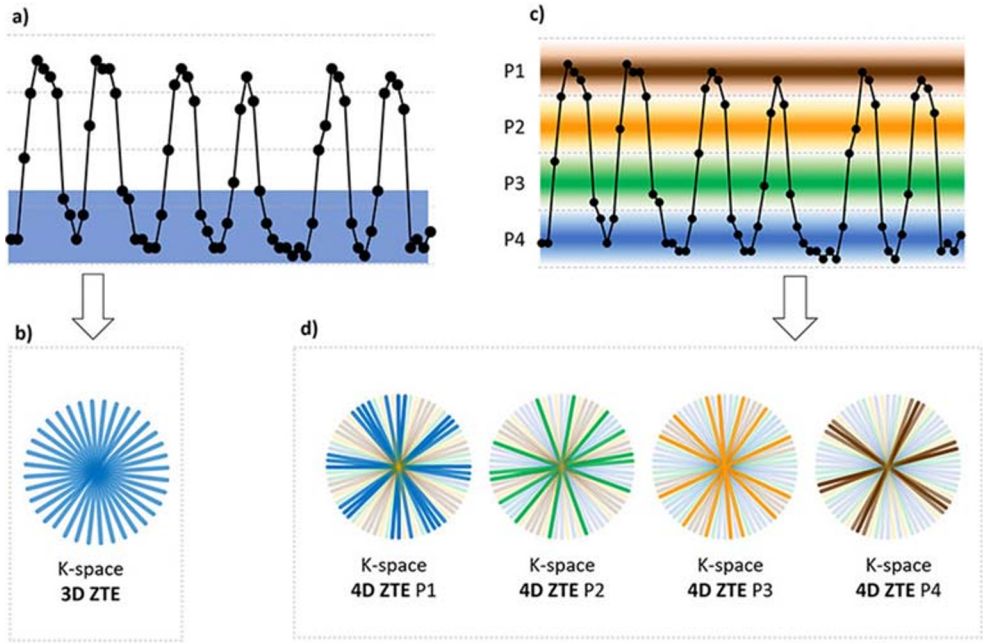

Fig. 2 Simplified illustration of respiratory-gated 3D ZTE and weighting applied 4D ZTE. **a**, **b** Signals from respiratory bellows. **b**, **d** Weighting-applied *k*-space data. For prospective respiratory gating in 3D ZTE, *k*-space spokes are acquired when the motion is within the acceptance window, i.e., the blue area in **a**. *k*-space spokes are equally weighted as shown in **b**. In 4D ZTE, *k*-space data along with physiological signals were collected during whole respiratory cycles. For each respiratory motion state, the ideal target signal was determined from physiological signals and weights, visualized as gradation per each color (**c**). It was determined by the distance between current data point and ideal target signal. The corresponding volume for each phase was reconstructed with weighted *k*-space data as shown in **d**. P1, phase 1; P2, phase 2; P3, phase 3; P4, phase 4

selecting a segmental bronchus perpendicular to the image plane, a circular ROI including the bronchial wall and luminal air was drawn on an image where the bronchus was delineated the best in each sequence.

Signal-to-noise ratios (SNRs) of lung parenchyma, trachea, peripheral bronchus, peripheral pulmonary vessel, aorta, subscapularis muscle, and lung nodule or mass were compared between the two sequences. Contrast-to-noise ratios (CNRs) of intrapulmonary structures including peripheral bronchus, peripheral pulmonary vessel, and lung nodule or mass were also compared. SNR was calculated as the mean SI of measuring structure/noise. The CNR was calculated as [mean SI (structure) − mean SI (lung)]/noise. The standard deviation of the SI in the tracheal lumen was considered as noise.

Qualitative evaluation

In a separate setting, two chest radiologists (with 23 years and 24 years of experience, respectively) independently evaluated axial and coronal images of 3D ZTE and 4D ZTE in a random order. Visualization of pulmonary vessels and bronchus, and sharpness of diaphragmatic contour as well as noise, artifacts,

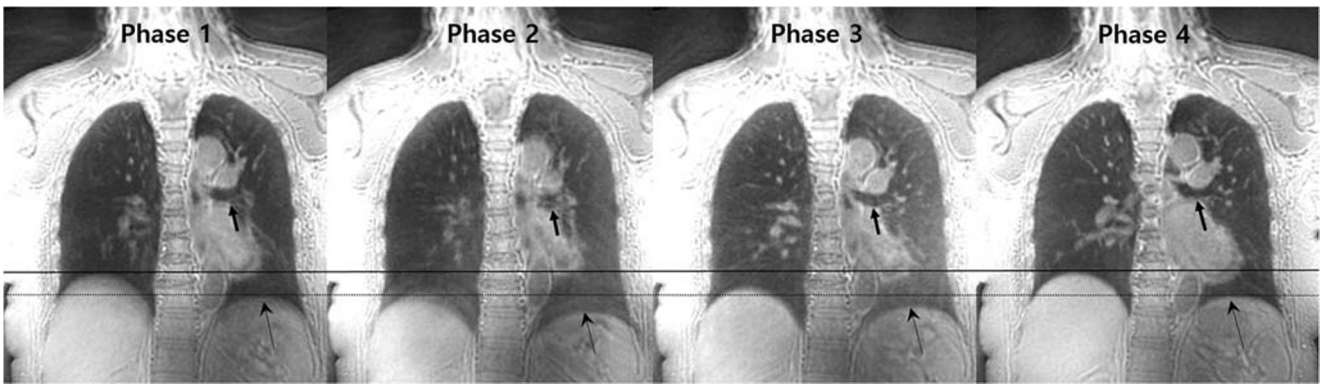

Fig. 3 Coronal 4D ZTE lung MR images in four different respiratory phases. Note different diaphragmatic positions in each phase. Arrows indicate left upper lobe bronchus (short arrows) and diaphragm (thin arrows). End-expiratory (phase 4) image demonstrates the best quality in delineating intrapulmonary structures and diaphragm

and overall diagnostic acceptability were scored. The score of each category was rated using a five-point scale as shown in Table 2.

Statistical analysis

The Wilcoxon signed-rank test was used to compare the differences in the SNR and CNR of normal structures and lung nodule or mass between 3D ZTE and 4D ZTE. The scores of subjective image quality between 3D ZTE and 4D ZTE were also compared using the Wilcoxon signed-rank test. Differences in image quality scores in 3D ZTE and 4D ZTE between the two groups (normal and low lung functions) were compared using the Mann-Whitney *U* test.

Inter-rater agreement for qualitative assessment was determined by calculating weighted kappa coefficient. The weighted kappa value was interpreted as follows: 0.20 or less, poor; 0.21–0.40, fair; 0.41–0.60, moderate; 0.61–0.80, substantial; and 0.81 or greater, almost perfect agreement. Statistical analyses were performed using SPSS package (version 22.0; SPSS Inc.). *P* values of less than 0.05 indicated statistical significance.

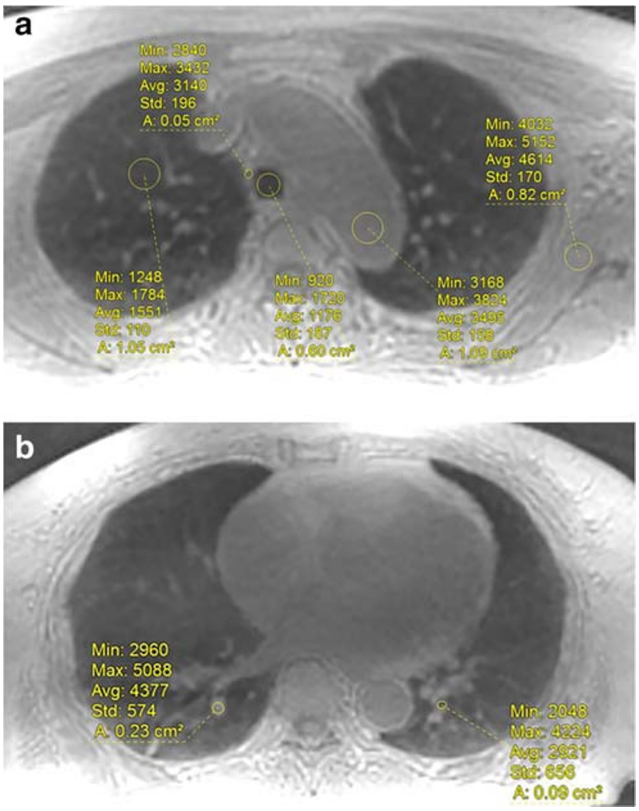

Fig. 4 An example of drawing regions of interest (ROIs) in lung parenchyma, the tracheal wall, tracheal lumen, aorta, and subscapularis muscle (**a**, from left to right) and peripheral pulmonary vessel and peripheral bronchus (**b**) in 4D ZTE. All measurements were performed three times. The same size was applied for the same location in 3D ZTE and 4D ZTE

Table 2 Qualitative scoring system of 3D and 4D ZTE lung MR images

Visualization of intrapulmonary vessels
1, unacceptable (indistinguishable segmental vessels)
2, poor (blurred visualization of segmental vessels)
3, fair (clear visualization of segmental vessels)
4, good (visualization of subsegmental vessels)
5, excellent (visualization of subsubsegmental vessels)
Visualization of the bronchus
1, unacceptable (indistinguishable lobar bronchus)
2, poor (visible lobar bronchus)
3, fair (visible segmental bronchus)
4, good (visible subsegmental bronchus)
5, excellent (visible subsubsegmental bronchus)
Sharpness of the diaphragm
1, transition width of diaphragm, ≥ 2 cm
2, 1 cm ≤ transition width of diaphragm < 2 cm
3, 0.5 cm ≤ transition width of diaphragm < 1 cm
4, transition width of diaphragm < 0.5 cm
5, sharply defined diaphragm
Noise and artifacts (cardiac, respiratory, and streaking)
1, unacceptable; 2, above-average noise/artifacts; 3, average and acceptable; 4, less than average; 5, minimum or nothing
Overall acceptability
1, unacceptable; 2, suboptimal; 3, satisfactory; 4, good; 5, excellent

Results

Image acquisitions using 3D ZTE and 4D ZTE sequences were successfully performed in all patients without any adverse events. The mean image acquisition time was 136 s (127–143 s) in 3D ZTE and 325 s (308–352 s) in 4D ZTE.

Table 3 Comparison of SNR and CNR of thoracic/intrapulmonary structures between 3D and 4D ZTE lung MR images

	3D ZTE	4D ZTE	*p* value
SNR			
Lung parenchyma	15.76 ± 3.06	24.72 ± 5.14	< 0.001*
Trachea	39.59 ± 7.51	62.84 ± 10.94	< 0.001*
Peripheral pulmonary vs.	34.78 ± 7.21	64.70 ± 12.76	< 0.001*
Peripheral bronchus	24.65 ± 5.70	48.65 ± 9.24	< 0.001*
Nodule/mass	53.36 ± 16.38	96.27 ± 27.11	< 0.001*
Aorta	36.75 ± 6.62	63.02 ± 11.56	< 0.001*
Muscle	53.47 ± 12.84	92.86 ± 15.74	< 0.001*
CNR			
Peripheral pulmonary vs.	19.02 ± 5.46	39.99 ± 10.37	< 0.001*
Peripheral bronchus	11.74 ± 4.50	29.89 ± 7.58	< 0.001*
Nodule/mass	37.25 ± 14.10	71.48 ± 24.03	< 0.001*

Data represent mean and standard deviation

*Difference is statistically significant

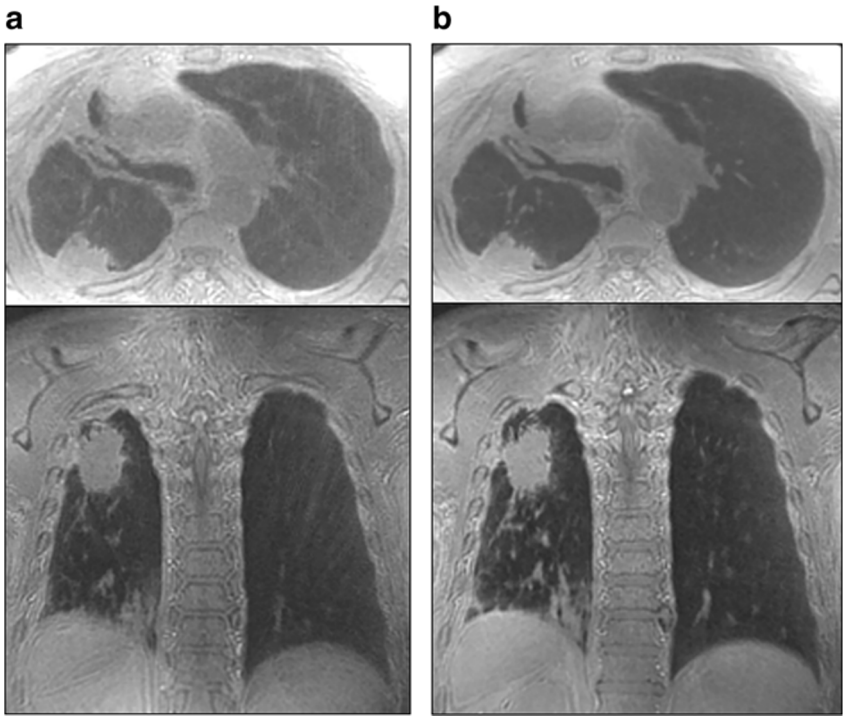

Fig. 5 The 3D ZTE (**a**) and 4D ZTE (**b**) images at end-expiration phase in a 72-year-old man with lung cancer. The patient manifested reduced lung function. Despite the use of hard gating, image blurring occurred frequently in 3D ZTE, especially near the diaphragm. The 4D ZTE images show sharply defined margin of the mass and diaphragms with less artifacts

Quantitative evaluation

When comparing end-expiratory images of 3D ZTE and 4D ZTE, the SNRs of lung parenchyma, trachea, peripheral bronchus, peripheral pulmonary vessel, aorta, muscle, and nodule/mass were significantly (all $p < 0.001$) higher in 4D ZTE. The CNRs of peripheral pulmonary vessel, peripheral bronchus, and nodule or mass were significantly higher in 4D ZTE (all $p < 0.001$) (Table 3).

Qualitative evaluation

The subjective image quality of intrapulmonary vessels and bronchi evaluated by two independent radiologists was significantly higher (all $p < 0.05$) in 4D ZTE (Fig. 5). Scores obtained by both readers for diaphragmatic sharpness, noise, artifacts, and overall acceptability in 4D ZTE were superior (all $p < 0.001$) to those in 3D ZTE (Table 4).

Inter-reader agreements in the evaluation of peripheral vessels (κ = 0.65 in 3D, $\kappa = 0.50$ in 4D), bronchus ($\kappa = 0.57$ in 3D, $\kappa = 0.66$ in 4D), diaphragm ($\kappa = 0.77$ in 3D, κ = 0.79 in 4D), image noise ($\kappa = 0.77$ in 3D, κ = 0.52 in 4D), artifacts ($\kappa = 0.69$ in 3D, $\kappa = 0.65$ in 4D), and overall acceptability ($\kappa = 0.63$ in 3D, $\kappa = 0.62$ in 4D) were substantial to moderate in both sequences.

In subgroup analysis of subjective image quality according to lung function, the image qualities were significantly (all, $p < 0.05$) different between the two groups with normal and low lung functions in 3D ZTE except for intrapulmonary vessels evaluated by reader 2 (Table 5). However, 4D ZTE did not

Table 4 Qualitative assessment of lung MR images obtained using 3D and 4D ZTE sequences by two independent readers (n = 21)

	Reader 1			Reader 2		
	3D ZTE	4D ZTE	p value	3D ZTE	4D ZTE	p value
Vessels	4.43 ± 0.68	4.86 ± 0.36	0.007*	4.19 ± 0.60	4.67 ± 0.48	0.004*
Bronchus	3.38 ± 0.97	4.33 ± 0.58	< 0.001*	3.38 ± 0.67	4.33 ± 0.58	< 0.001*
Diaphragm	2.62 ± 0.97	4.29 ± 0.64	< 0.001*	2.86 ± 0.91	4.43 ± 0.67	< 0.001*
Noise	3.00 ± 1.00	4.38 ± 0.67	< 0.001*	3.05 ± 0.92	4.57 ± 0.51	< 0.001*
Artifacts	3.14 ± 1.12	4.19 ± 0.87	< 0.001*	3.24 ± 1.04	4.38 ± 0.67	< 0.001*
Overall acceptability	3.14 ± 1.11	4.29 ± 0.78	< 0.001*	3.38 ± 1.02	4.38 ± 0.67	< 0.001*

Data are mean and standard deviation

*Difference is statistically significant

Table 5 Comparison of image quality scores of 3D and 4D ZTE lung MRI between patients with normal and low lung functions

	Reader 1						Reader 2					
	3D ZTE			4D ZTE			3D ZTE			4D ZTE		
	Normal LF ($n = 12$)	Low LF ($n = 9$)	p value	Normal LF ($n = 12$)	Low LF ($n = 9$)	p value	Normal LF ($n = 12$)	Low LF ($n = 9$)	p value	Normal LF ($n = 12$)	Low LF ($n = 9$)	p value
Vessels	4.75 ± 0.45	4.00 ± 0.71	0.012*	4.92 ± 0.29	4.78 ± 0.44	0.380	4.42 ± 0.52	3.89 ± 0.60	0.052	4.67 ± 0.50	4.67 ± 0.50	1.0
Bronchus	3.92 ± 0.90	2.67 ± 0.50	0.003*	4.42 ± 0.67	4.22 ± 0.44	0.348	3.67 ± 0.65	3.00 ± 0.50	0.022*	4.33 ± 0.65	4.33 ± 0.50	0.903
Diaphragm	3.00 ± 0.95	2.11 ± 0.78	0.034*	4.33 ± 0.65	4.22 ± 0.67	0.692	3.17 ± 0.94	2.44 ± 0.73	0.048*	4.42 ± 0.67	4.44 ± 0.73	0.874
Noise	3.42 ± 0.90	2.44 ± 0.88	0.025*	4.50 ± 0.67	4.22 ± 0.67	0.306	3.42 ± 0.67	2.56 ± 1.01	0.043*	4.58 ± 0.52	4.56 ± 0.53	0.901
Artifacts	3.75 ± 0.97	2.33 ± 1.00	0.006*	4.50 ± 0.80	3.78 ± 0.83	0.055	3.75 ± 0.87	2.56 ± 0.88	0.009*	4.50 ± 0.67	4.22 ± 0.67	0.306
Overall acceptability	3.67 ± 0.99	2.44 ± 0.88	0.012*	4.42 ± 0.79	4.11 ± 0.78	0.335	3.83 ± 0.84	2.78 ± 0.97	0.022*	4.50 ± 0.67	4.22 ± 0.67	0.306

Data are mean and standard deviation

LF lung function

*Difference is statistically significant

show any difference between the two groups. The overall acceptability of images in 3D ZTE was acceptable (satisfactory or better, score ≥ 3) in 10 to 11 of 12 patients with normal lung function by two readers. Among 9 patients with low lung function, the 3D ZTE images of 4 patients were considered acceptable by both readers. The 4D ZTE images were acceptable for all patients by both readers in both groups.

Generation of dynamic images in 4D ZTE

In 4D ZTE, using images derived from multiple respiratory phases, dynamic breathing MR images were generated. Diaphragmatic motion and changes in airway dimension during the respiratory cycle were identified in dynamic images (Supplementary Fig. 1).

Discussion

Since gradient is already turned on when the RF pulse is applied and gradient switching is avoided, loss of short-lasting signals can be minimized in ZTE, facilitating signal acquisition from tissues with extremely short T2 values [10]. Minimal gradient variations in ZTE lead to a dramatic decrease in acoustic noise and patient annoyance [17]. The feasibility and potential of ZTE for lung parenchymal imaging have been explored in clinical studies [11, 12]. Notwithstanding advances in imaging techniques, respiratory motion artifacts remain a major challenge for lung MRI. Motion artifacts appear as blurring, ghosting, signal dropouts, and undesirable signal enhancement [18]. To obtain respiratory motion–resolved lung MR images, we used the 4D technique in ZTE sequence. Our results based on 4D ZTE demonstrated improved respiratory motion compensation in all patients. While 4D ZTE showed consistent image qualities regardless of patients' lung function, 3D ZTE showed significantly inferior image quality in patients with low lung function compared with patients manifesting normal lung function. The 3D ZTE images were acceptable in 83% (10/12) and 92% (11/12) by two readers in the normal lung function group. The 3D ZTE images were acceptable in 44% (4/9) by each of the two readers in the low lung function group. The 4D ZTE images were acceptable in 100% by each of two readers in both normal and low lung function groups.

In 3D ZTE and 4D ZTE imaging, different respiratory gating techniques were applied. The 3D ZTE used a prospective gating technique, which is a commonly used respiratory motion compensation method in clinical setting. In 4D ZTE, a retrospective soft gating technique was used and data acquisition was performed continuously during whole respiratory cycles. In prospective gating, data collection is performed within a limited window around a reference position, usually end-expiration, because patients' breathing pattern is most

consistent and the breathing time is longer in this phase [19]. Despite the use of gating, image blurring occurred routinely in 3D ZTE, especially near the diaphragm. Because a few motions in an acquisition window are not considered in reconstruction, images with poor motion compensation were obtained in patients with inconsistent respiratory patterns [20–22]. Soft gating techniques have shown promise for reconstructing high-resolution, motion-robust MR images [23, 24]. In the present study, motion compensation using soft gating in 4D ZTE was accomplished by giving different weights on signals depending on the variations between actual signal and ideal target signal in each phase. The 4D ZTE images at end-expiratory phase demonstrated better SNR and CNR of normal structures and nodules compared with 3D ZTE, due to higher signal and lower noise of 4D ZTE images owing to reduced motion within voxels. By using all data obtained during whole respiratory cycle, 4D ZTE substantially reduced the artifacts due to under-sampling.

Acquisition time of 4D ZTE images was longer than that of 3D ZTE (mean, 325 s vs. 127 s). The 3D ZTE is more efficient than 4D ZTE when the scan time for structural lung imaging is considered in patients with normal lung function. However, the scan time for 4D ZTE was comparable to other free-breathing lung MR sequences [24, 25]. Any additional efforts were not required for patients or operators in 4D ZTE compared with 3D ZTE. In addition, dynamic respiratory images were generated using the pooled volume data from multiple phases, which potentially yielded functional information such as dynamic changes of airway dimension, lung volume, and diaphragmatic motion [15]. Therefore, the use of 4D ZTE in routine chest MR facilitates acquisition of simultaneous motion-robust lung images and dynamic motion information regardless of patients' respiratory performance in 5 min.

High-resolution images of 4D ZTE MR may be useful for the evaluation of pulmonary parenchymal status, potentially obviating chest CT scans, especially in patients who are vulnerable to radiation exposure. As demonstrated by recent lung MR studies using UTE, 4D ZTE represents another promising tool providing simultaneous structural and functional information in various diseases without contrast administration [13, 15, 26].

This study has several limitations. First, this study included a small number of patients. Further studies with larger populations are required to corroborate our results and improve data quality. Second, we evaluated the image quality of 4D ZTE compared with that of 3D ZTE using different gating techniques. The 3D ZTE is a product system, and prospective gating used in 3D ZTE is a standard method for the compensation of respiratory motion in clinical MRI. However, 4D ZTE using soft gating is a new technique developed specifically to improve image quality and applicability of ZTE sequence in lung MRI. Therefore, the performance and benefits of 4D ZTE were assessed via comparison with 3D ZTE. Third, using non-ECG-gated scan protocols, cardiac motion could have affected the image quality, although not as much as respiratory motion. Fourth, the image quality of respiratory phases other than end-expiration should be substantially improved. A dynamic MRI entails increasing the number of phases and improving reconstruction techniques. Lastly, the ZTE sequence and respiration motion correction software may not be available in other MR machines. A substantial improvement of the sequence for other machines is needed to provide benefits for patients with lung disease exposed to ionizing techniques.

In conclusion, this study demonstrated the feasibility of free-breathing 4D ZTE lung imaging under clinical settings. The 4D ZTE generated respiratory motion–resolved lung parenchymal images with high SNR and CNR without being affected by patients' lung function or respiratory performance. The 4D ZTE also has the potential to extend lung MR application by providing functional information via dynamic respiratory imaging.

Acknowledgments GE Healthcare provided authors with 4D ZTE research pulse. However, GE Healthcare had no role in the design or performance of the study, data analyses, or data interpretation.

Funding information This research was supported by the Dasol Life Science Research Fund.

Compliance with ethical standards

Guarantor The scientific guarantor of this publication is Kyung Nyeo Jeon.

Conflict of interest The authors of this manuscript declare relationships with the company GE Healthcare. MJ Hwang, JS Lee, and Anne Menini are employees of GE Healthcare.

Statistics and biometry No complex statistical methods were necessary for this paper.

Informed consent Written informed consent was obtained from all patients in this study.

Ethical approval This study was approved by the Institutional Review Board of Gyeongsang National University Changwon Hospital.

Methodology
- prospective
- observational
- performed at one institution

References

1. Garwood M (2013) MRI of fast-relaxing spins. J Magn Reson 229: 49–54

2. Kuethe DO, Adolphi NL, Fukushima E (2007) Short data-acquisition times improve projection images of lung tissue. Magn Reson Med 57:1058–1064
3. Ohno Y, Koyama H, Yoshikawa T et al (2016) Pulmonary high-resolution ultrashort TE MR imaging: comparison with thin-section standard- and low-dose computed tomography for the assessment of pulmonary parenchyma diseases. J Magn Reson Imaging 43: 512–532
4. Willmering MM, Robison RK, Wang H, Pipe JG, Woods JC (2019) Implementation of the FLORET UTE sequence for lung imaging. Magn Reson Med 82:1091–1100
5. Torres L, Kammerman J, Hahn AD et al (2019) Structure-function imaging of lung disease using ultrashort echo time MRI. Acad Radiol 26:431–441
6. Bergin CJ, Pauly JM, Macovski A (1991) Lung parenchyma: projection reconstruction MR imaging. Radiology 179:777–781
7. Togao O, Tsuji R, Ohno Y, Dimitrov I, Takahashi M (2010) Ultrashort echo time (UTE) MRI of the lung: assessment of tissue density in the lung parenchyma. Magn Reson Med 64:1491–1498
8. Ma W, Sheikh K, Svenningsen S et al (2015) Ultra-short echo-time pulmonary MRI: evaluation and reproducibility in COPD subjects with and without bronchiectasis. J Magn Reson Imaging 41:1465–1474
9. Gai ND, Malayeri A, Agarwal H, Evers R, Bluemke D (2016) Evaluation of optimized breath-hold and free-breathing 3D ultrashort echo time contrast agent-free MRI of the human lung. J Magn Reson Imaging 43:1230–1238
10. Weiger M, Brunner DO, Dietrich BE, Muller CF, Pruessmann KP (2013) ZTE imaging in humans. Magn Reson Med 70:328–332
11. Gibiino F, Sacolick L, Menini A, Landini L, Wiesinger F (2015) Free-breathing, zero-TE MR lung imaging. MAGMA 28:207–215
12. Bae K, Jeon KN, Hwang MJ et al (2019) Comparison of lung imaging using three-dimensional ultrashort echo time and zero echo time sequences: preliminary study. Eur Radiol 29:2253–2262
13. Dournes G, Menut F, Macey J et al (2016) Lung morphology assessment of cystic fibrosis using MRI with ultra-short echo time at submillimeter spatial resolution. Eur Radiol 26:3811–3820
14. Forman C, Piccini D, Grimm R, Hutter J, Hornegger J, Zenge MO (2015) Reduction of respiratory motion artifacts for free-breathing whole-heart coronary MRA by weighted iterative reconstruction. Magn Reson Med 73:1885–1895
15. Feng L, Delacoste J, Smith D et al (2019) Simultaneous evaluation of lung anatomy and ventilation using 4D respiratory-motion-resolved ultrashort echo time sparse MRI. J Magn Reson Imaging 49:411–422
16. Menini A, Lai P, McKinnon G, Wiesinger F (2018) Self-calibrated soft gating for respiratory resolved 3D+ time lung ZTE. Proceedings of the joint annual meeting ISMRM-ESMRMB, Paris, France. Available via http://archive.ismrm.org/2018/4104.html. Accessed 19 Nov 2019
17. Costagli M, Symms MR, Angeli L et al (2016) Assessment of silent T1-weighted head imaging at 7 T. Eur Radiol 26:1879–1888
18. Zaitsev M, Maclaren J, Herbst M (2015) Motion artifacts in MRI: a complex problem with many partial solutions. J Magn Reson Imaging 42:887–901
19. Liu C, Alessio A, Pierce L et al (2010) Quiescent period respiratory gating for PET/CT. Med Phys 37:5037–5043
20. Scott AD, Keegan J, Firmin DN (2009) Motion in cardiovascular MR imaging. Radiology 250:331–351
21. Ehman RL, McNamara MT, Pallack M, Hricak H, Higgins CB (1984) Magnetic resonance imaging with respiratory gating: techniques and advantages. AJR Am J Roentgenol 143:1175–1182
22. Nehrke K, Bornert P, Manke D, Bock JC (2001) Free-breathing cardiac MR imaging: study of implications of respiratory motion–initial results. Radiology 220:810–815
23. Johnson KM, Block WF, Reeder SB, Samsonov A (2012) Improved least squares MR image reconstruction using estimates of k-space data consistency. Magn Reson Med 67:1600–1608
24. Jiang W, Ong F, Johnson KM et al (2018) Motion robust high resolution 3D free-breathing pulmonary MRI using dynamic 3D image self-navigator. Magn Reson Med 79:2954–2967
25. Rank CM, Heußer T, Buzan MT et al (2017) 4D respiratory motion-compensated image reconstruction of free-breathing radial MR data with very high undersampling. Magn Reson Med 77:1170–1183
26. Ohno Y, Koyama H, Yoshikawa T et al (2017) Standard-, reduced-, and no-dose thin-section radiologic examinations: comparison of capability for nodule detection and nodule type assessment in patients suspected of having pulmonary nodules. Radiology 284:562–573

Publisher's note Springer Nature remains neutral with regard to jurisdictional claims in published maps and institutional affiliations.